

# EARTHQUAKE DAMAGE ASSESSMENT FOR RC PIERS BY TIME-FREQUENCY ANALYSIS CONSIDERING ENTIRE BRIDGE

\*Aiko Furukawa<sup>1</sup>, Yuta Kawamatsu<sup>2</sup>

<sup>1</sup>Department of Urban Management, Kyoto University, Japan

\*Corresponding Author, Received: 15 July 2023, Revised: 22 Aug. 2023, Accepted: 5 Sept. 2023

**ABSTRACT:** In this study, the previously proposed earthquake damage assessment method for reinforced concrete (RC) piers was verified through seismic response analysis of an entire bridge. The method measures the acceleration histories at the bottom and top of the pier during earthquakes to estimate the ratio of the initial natural frequency to the lowest natural frequency during earthquakes using time-frequency analysis since it is related to earthquake damage. The previous study verified the method through numerical analysis and shaking table test results of a single pier. However, since the actual pier is connected to the adjacent pier and abutment via the girder, it is important to consider the dynamics of the entire bridge. Therefore, this study verified the method through numerical analysis of the entire bridge. It was found that the method can detect damage to each pier when accelerations in the bridge axis direction are used because the natural frequency only changes for a damaged pier. On the other hand, the method cannot detect which pier is damaged and can only detect if any piers are damaged when accelerations in the direction perpendicular to the bridge axis are used since the natural frequency changed even for undamaged piers. It was verified that the difference between the two directions was caused due to the constraint conditions of the bearings.

*Keywords: Earthquake Damage Assessment, RC Pier, Time-Frequency Analysis, Entire Bridge*

## 1. INTRODUCTION

Road bridges are important in rescue and restoration activities after earthquakes. Therefore, a quick assessment of bridge damage after earthquakes is necessary. The damage is often inspected visually. However, inspecting damage visually at night or in bad weather conditions is difficult. Furthermore, the more extensive the damage, the more time and human resources are required for visual inspection.

Regarding the restoration of road facilities, in the 2004 Niigata Chuetsu-Oki Earthquake, there was an area where it took about a week until the traffic restrictions were lifted [1]. Also, road closures occurred in the 2016 Kumamoto earthquake, and emergency restoration took time due to the lack of necessary materials and equipment [2]. The importance of reducing the time required to restore the functions of road networks has been reaffirmed. Therefore, prompt earthquake damage assessment is important for rescue and restoration activities.

Many earthquake damage assessment methods for bridge piers have been proposed. Most simple methods use changes in natural frequencies before and after the earthquake [3-5]. Only two-time measurement of pre- and post-earthquake is required. However, since the natural frequency recovers after the earthquake, the methods using the natural frequency after the earthquake underestimates the damage. Therefore, methods

based on real-time measurement have been proposed [6,7]. A method of estimating the maximum ductility factor of the pier using real-time input and response acceleration measurement has been proposed [6]. However, the method assumes the nonlinear characteristics of the pier, so the application is limited. A wavelet-transform-based damage detection method also has been proposed [7]. The method can detect damage occurrence, but estimating the damage degree is difficult.

The authors proposed an earthquake damage assessment method that measures the input and response acceleration in real time during the earthquake [8]. The method detects damage using the ratio of the natural frequency before the earthquake to the lowest natural frequency during the earthquake based on the time-frequency analysis. The shaking table tests showed that the natural frequency of the pier decreases due to damage during an earthquake but gradually recovers after the earthquake and that the lowest natural frequency has a higher correlation with the degree of damage than the natural frequency after the earthquake. This suggests that measuring natural frequencies in real time is important. The authors have further developed the research and proposed a method to identify the damage indices that are highly correlated with damage [9].

So far, the validity of the author's damage assessment method has been verified by numerical analysis and shaking table tests on single-pier

models. However, piers are connected to adjacent piers and abutments by girders. Therefore, the damaged piers may affect the response of adjacent undamaged piers. This study aims to validate the author's damage assessment method for bridge piers by conducting a seismic response analysis of the entire bridge. The effect of damaged piers on the adjacent undamaged piers is investigated by focusing on the constraint conditions of the bearings between the piers and the girder.

## 2. RESEARCH SIGNIFICANCE

Most studies on earthquake damage assessment methods for bridge piers focus on single piers and do not consider the dynamics of the entire bridge. However, the dynamics of piers when only the piers are modeled differ from those when the entire bridge is modeled. The significance of this study is to focus on the effect of the dynamics of the entire bridge on the damage assessment method for a single pier. This study revealed that the constraint conditions of the bearings between the pier and the girder influence the results, and the method shows different performance between the bridge axis direction and the direction perpendicular to the bridge axis.

## 3. DAMAGE ASSESSMENT METHOD

This section describes the previously proposed damage assessment method for RC piers [8]. As shown in Fig.1, a structure consists of a footing, a pier, and a girder. Two acceleration sensors are installed on the footings and girders to measure horizontal accelerations. The acceleration of the footing is defined as an input acceleration, and the acceleration of the girder is defined as a response acceleration. The procedure of the method is as follows. In step 1, input and response accelerations are measured during an earthquake. In step 2, the method computes the short-time Fourier transforms (STFT) of the accelerations. In Fig.1, the upper and middle graphs on the right side are the STFT of the response and input accelerations. In step 3, the method computes the short-time transfer function (STTF) by dividing the STFT of the response acceleration by the STFT of the input acceleration. The STTF is normalized so that the maximum value becomes 1 for each time step. The lower right graph in Fig.1 shows the normalized STTF (NSTTF), where blue indicates 0 and red indicates the maximum value 1. By tracing the maximum value of the NSTTF (red color), the transition of the natural frequency of the pier can be captured. The natural frequency decreases to the lowest value of  $F_A$  due to damage and then recovers to  $F_B$  after the earthquake. In step 4, the method extracts the natural frequency before the

earthquake  $F_0$  (intact state), the lowest natural frequency during the earthquake  $F_A$  from the NSTTF. The method relates  $(F_0/F_A)^2$  to the damage-related index (maximum displacement).

The previous study [8] revealed that when the pier suffers slight damage, it is difficult to detect damage using  $F_B$  since it recovers as high as  $F_0$ . Even in such a case, damage could be detected using  $F_A$ . Moreover, the possibility was found that the maximum displacement can be estimated from  $(F_0/F_A)^2$ . The relationship between  $(F_0/F_A)^2$  and the maximum displacement is obtained, as shown in Fig.2 in the previous study [8] using the shaking table test result [10], in which amplitude-adjusted accelerations were input. The notation "a%(n)" in Fig.2 indicates that this is the n-th experiment using an acceleration waveform whose amplitude was adjusted by a factor of a (%). As shown in Fig.2, a monotonically increasing relationship exists between  $(F_0/F_A)^2$  and the maximum displacement. The maximum displacement is an indicator of the degree of damage. By mapping the relationship between  $(F_0/F_A)^2$  and the maximum displacement through numerical analysis a priori, we can estimate the maximum response displacement from  $(F_0/F_A)^2$  during an earthquake.

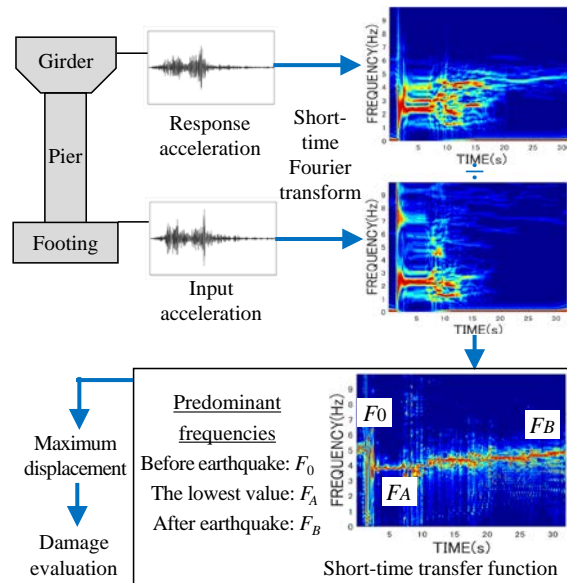


Fig. 1. Procedure of damage assessment method

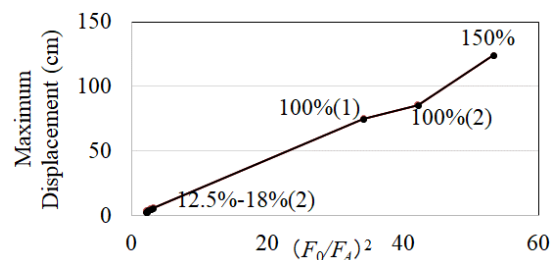


Fig.2 Relationship between  $(F_0/F_A)^2$  and maximum displacement [8]

#### 4. ANALYSIS MODEL OF ENTIRE BRIDGE

##### 4.1 Overview

The method shown in Fig. 1 is developed based on the results of shaking table tests and numerical analysis on single piers. However, actual piers are connected to adjacent piers and abutments by girders, so it is necessary to consider the effect of the dynamics of the entire bridge. This study aims to verify the damage assessment method through the numerical analysis of the entire bridge.

##### 4.2 Analysis Model

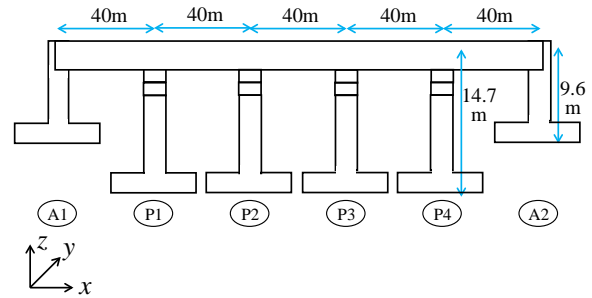
A schematic diagram of the entire bridge is shown in Fig.3(a). It is a 5-span continuous steel girder bridge [11]. The x-axis is the bridge axis, the y-axis is horizontal and perpendicular to the bridge axis, and the z-axis is vertical. All degrees of freedom at the base of the foundation were fixed.

Figure 3(b) shows the abutment and footing, and Fig.3(c) shows the pier and footing. Figure 3(d) shows the analytical model of the entire bridge. The abutments, piers, footings, and girders are modeled with beam elements, and the bearings are modeled with spring elements. Yellow circles indicate nodes. In Figs. 3(c) and 3(d), only three nodes (top, middle, and bottom) are shown for each pier for simplicity. The actual model divides the piers into eight elements in the lower half and four in the upper half. Similarly, the girders are divided into eight elements per span. The springs representing the bearings have no height, so both ends of the bearings have the same height.

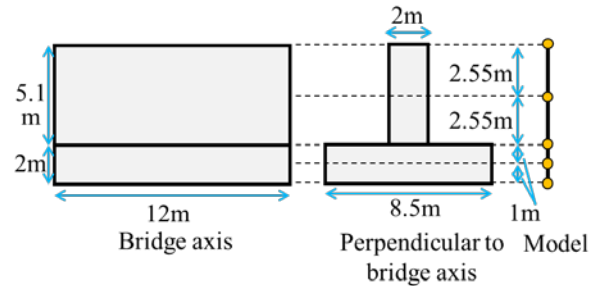
The bearings are assumed to be rubber bearings. The girder is elastically supported by the bearings on both abutments and piers in the bridge axis direction (x-axis). The girder is restrained by the bearings on the abutments, and the girder is elastically supported by the bearings on the piers in the direction perpendicular to the bridge axis (y-axis). The girder is restrained by the bearing in the vertical direction (z-axis) and the rotational direction around the x-axis and is not restrained by the bearing in the rotational direction around the y-axis and z-axis. The spring constants of the bearings are shown in Table 1.

The material properties are set as follows. Young's modulus of the abutments and piers was set to  $2.0 \times 10^7$  kN/m<sup>2</sup> and unit volume mass to 2.5 ton/m<sup>3</sup>. Young's modulus of the footings was set to  $2.0 \times 10^8$  kN/m<sup>2</sup>, which is greater than that of the abutments and piers, and the unit volume mass was set to 2.5 ton/m<sup>3</sup>. The girders are steel with axial stiffness of 6.82 kN, bending stiffness around the y-axis of  $4.77 \times 10^7$  kN/m<sup>2</sup>, bending stiffness around the z-axis of 5.69 kN/m<sup>2</sup>, torsional moment of  $6.00 \times 10^7$  kN/m<sup>2</sup> and mass per unit length of

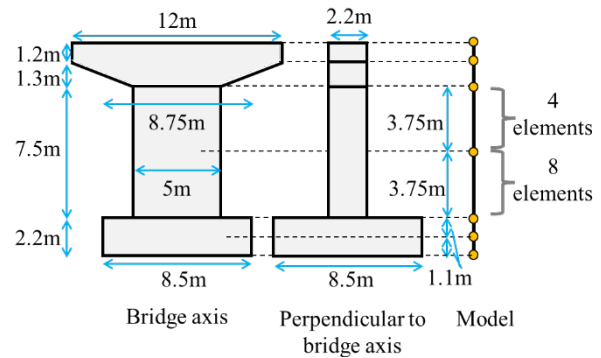
14.7 ton. The damping constants for each member are set, as shown in Table 2.



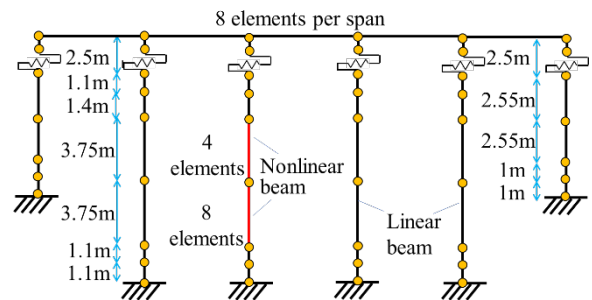
(a) Schematic diagram of the entire bridge



(b) Abutment



(c) Pier



(d) Analysis model

Fig.3 Target bridge

Table 1 Spring constant of bearings (kN/m)

| Direction                        | Abutment           | Pier                |
|----------------------------------|--------------------|---------------------|
| Bridge axis (x)                  | $8.36 \times 10^3$ | $2.408 \times 10^4$ |
| Perpendicular to bridge axis (y) | Fixed              | $2.408 \times 10^4$ |

### 4.3 Nonlinear Characteristics of Pier

The P2 pier, shown in red in Fig.3(d), is modeled with nonlinear elements, and the other elements are set linear. This study confirms whether the damage to the P2 pier can be detected. The moment-curvature relationship of the nonlinear elements is modeled using the Takeda model [12] shown in Fig. 4, and the parameters for the Takeda model are shown in Table 3.  $K_r$  is the unloading stiffness after yielding occurred.  $K_y$  is the stiffness between the crack and yield point on the opposite sign side of the curvature.  $\varphi_m$  is the maximum curvature, and  $\varphi_y$  and  $\varphi_c$  are the curvature when yielding and crack occur.

### 4.4 Results of Eigenvalue Analysis

#### 4.4.1 Bridge Axis Direction (x)

Figure 5 shows the mode shape in the axial direction (x). The vibration of different members is dominant for each mode. In the 1<sup>st</sup>, 2<sup>nd</sup>, and 5<sup>th</sup> modes, the vibration of the bearing, girder, and abutments is dominant, respectively. In the 3<sup>rd</sup> and 4<sup>th</sup> modes, the vibration of the P1 and P4 piers and that of the P2 and P3 piers are dominant, respectively. Since the 1<sup>st</sup>, 3<sup>rd</sup>, and 4<sup>th</sup> modes have large participation factors and the 3<sup>rd</sup> and 4<sup>th</sup> modes have the same natural frequency, the Rayleigh damping was set using these modes.

#### 4.4.2 Direction perpendicular to the bridge axis (y)

Figure 6 shows the mode shapes in y direction.

Table 2 Damping factor of members

|                               |      |
|-------------------------------|------|
| Girder                        | 0.02 |
| Bearing                       | 0.03 |
| Abutment / Pier (Linear beam) | 0.05 |
| Pier (Nonlinear beam)         | 0.02 |
| Footing                       | 0.2  |

Table 3 Parameters of the Takeda model

| Direction | $a_1$                 | $a_2$                 | $\varphi_c$           | $\varphi_y$           |
|-----------|-----------------------|-----------------------|-----------------------|-----------------------|
| x         | 0.182                 | $4.06 \times 10^{-4}$ | $8.62 \times 10^{-5}$ | $1.04 \times 10^{-3}$ |
| y         | $7.32 \times 10^{-3}$ | $1.05 \times 10^{-3}$ | $3.89 \times 10^{-5}$ | $4.01 \times 10^{-4}$ |

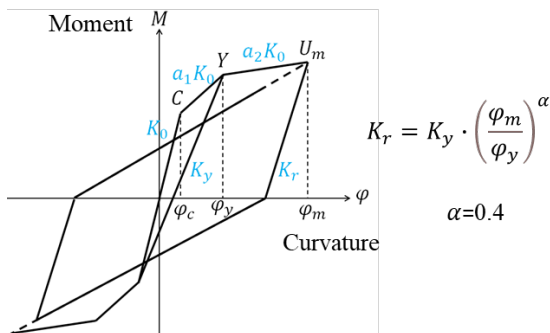


Fig.4. Takeda model (Trilinear model)

The 3<sup>rd</sup>, 4<sup>th</sup>, 6<sup>th</sup>, and 7<sup>th</sup> modes are the modes where the vibration of the piers is dominant. Since the 3<sup>rd</sup> and 7<sup>th</sup> modes have large participation factors, the Rayleigh damping was set using these two modes.

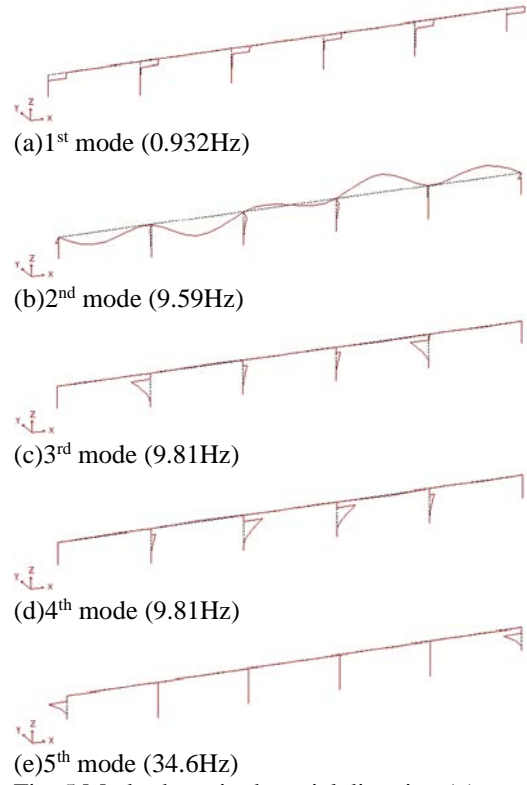


Fig. 5 Mode shape in the axial direction (x)

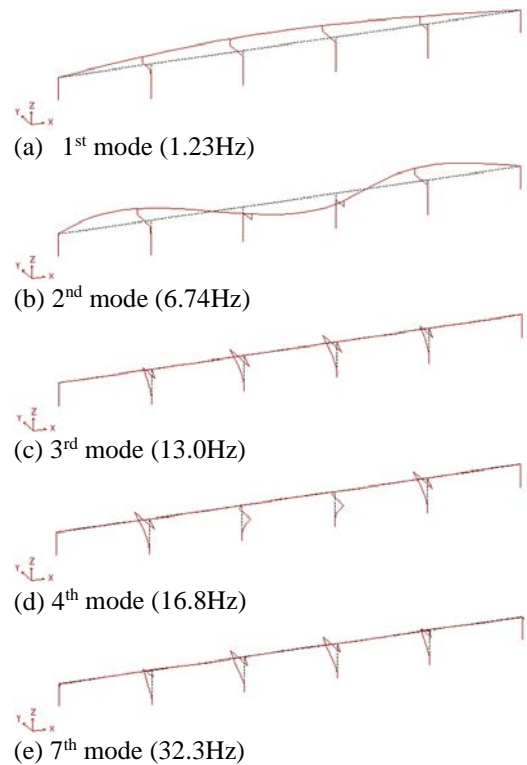


Fig. 6 Mode shape in the direction perpendicular to the bridge axis (y)

## 5. VALIDATING DAMAGE ASSESSMENT METHOD BY SEISMIC RESPONSE ANALYSIS OF ENTIRE BRIDGE

### 5.1 Overview

A seismic response analysis of the entire bridge was conducted, and the NSTTF (normalized short-time transfer function) was obtained for each pier. The initial natural frequency  $F_0$  and the lowest natural frequencies during earthquake  $F_A$  are estimated, and the relationship between  $(F_0/F_A)^2$  and the maximum displacement is examined.

### 5.2 Input ground motion and time integration

Three design ground motions for interplate earthquakes (Type I-I-1, I-II-1, I-III-1) and three design ground motions for inland earthquakes (Type II-I-1, II-II-1, II-III-1) defined in the design specification for the highway bridge are input [13]. The acceleration amplitude was adjusted by multiplying 0.2 and 1 to consider the small and large earthquakes. Therefore, a total of 12 ground motions are considered. The acceleration waveform of Type I-I-1 is shown in Fig.7. As for time integration, Newmark  $\beta$  method ( $\beta = 0.25$ ) was used. A time interval of 0.001 s was used.

### 5.3 Time-frequency analysis

The input and response accelerations are required to obtain the NSTTF. The acceleration responses of the nodes at the base and the top of the pier were used. Following a previous study [8], the short-time Fourier transform was computed using a rectangular window function with a time width of 5.0 s, and smoothing was performed in the frequency domain using a Parzen window with a frequency width of 0.2 Hz.

### 5.4 Results in bridge direction (x)

#### 5.4.1 NSTTF

Since the same tendency was observed for the twelve ground motions, the NSTTFs for Type I-I-1 are shown in Fig.8 as an example. The P2 pier cracked when the ground motion amplitude was multiplied by 0.2 and yielded when multiplied by 1.0. The other piers are linear, so no damage occurs to these piers. The left graphs are for the P1 pier, and the right graphs are for the P2 pier. The initial natural frequencies of both piers are 9.81 Hz, the 3<sup>rd</sup> and 4<sup>th</sup> mode natural frequencies. In both amplitude levels, the natural frequencies of the P1 pier remained constant. On the other hand, the natural frequency of the P2 pier decreased, and the decrease in the natural frequency was greater for the case with an amplitude multiplied by 1.0.

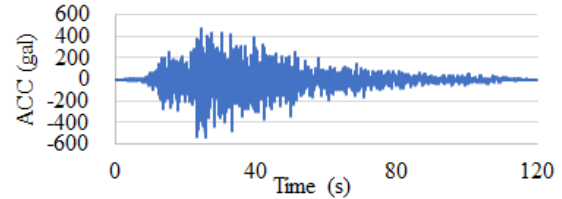
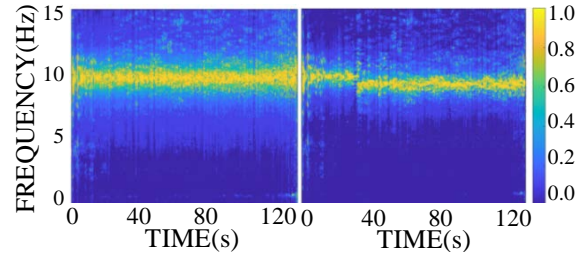
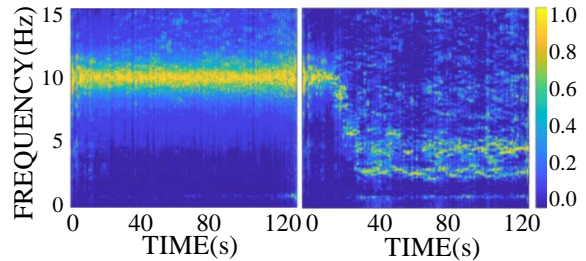


Fig.7 Input ground motion (Type I-I-1)



(a) Type I-I-1 multiplied by 0.2



(b) Type I-I-1 multiplied by 1

Fig.8 NSTTF in the bridge direction (Left: P1 pier, Right: P2 pier)

In the bridge direction, only the NSTTF of the damaged pier shows a reduction in natural frequency, so it is possible to know which piers have been damaged using the NSTTF.

#### 5.4.2 Eigenvalue analysis corresponding to the lowest natural frequencies of P2 pier

In the case with an amplitude of 1x (Fig. 8(b)), the lowest natural frequency for the P2 pier is around 3 Hz, while that for the P1 pier is a constant of 9.81 Hz. The bending stiffness of the P2 pier corresponds to the lowest natural frequency during the earthquake  $EI_d$  is estimated using the moment-curvature relationship shown in Fig. 9 as follows.

$$EI_d = \frac{M_{max} - M_{min}}{\varphi_{max} - \varphi_{min}} \quad (1)$$

$M_{max}$  and  $M_{min}$  are the maximum and minimum bending moments.  $\varphi_{max}$  and  $\varphi_{min}$  are the curvature at the maximum and minimum bending moments.

The eigenvalue analysis using the bending stiffness of the P2 pier shown in Eq. (1) is conducted to examine the lowest natural frequency. Figs.10(a) and (b) show the 2<sup>nd</sup> and 4<sup>th</sup> mode shapes. In 2<sup>nd</sup> mode (3.22 Hz), the vibration of the P2 pier is dominant. In the 4<sup>th</sup> mode (9.81 Hz), the vibration of P1, P3, and P4 piers is dominant.

Before the earthquake, the vibration of P2 and P3 is dominant in the 3<sup>rd</sup> mode (Fig. 5(c), 9.81Hz), and the vibration of P1 and P4 is dominant in the 4<sup>th</sup> mode (Fig. 5(d), 9.81Hz).

It is found that the natural frequency for the P1, P3, and P4 piers does not change, and the NSTTF for the P1 pier captured this phenomenon. The natural frequency for the P2 pier only changed to 3.22 Hz, and the NSTTF for the P2 pier captured this phenomenon.

### 5.5 Results perpendicular to bridge direction (y)

#### 5.5.1 NSTTF

Since the same tendency was observed for the twelve ground motions, the NSTTF for all piers for I-I-1 when the ground motion amplitude is multiplied by 1.0 are shown in Fig.11 as an example. In the NSTTF for the damaged P2 pier, the natural frequency decreases from about 13 Hz to about 10 Hz. However, the natural frequencies of the other undamaged piers also changed, from about 13 Hz to about 10 Hz and about 14 Hz for the P1 and P3 piers and increasing to about 14 Hz for the P4 pier. The reason for this is verified by an eigenvalue analysis that considers the reduced bending stiffness during the earthquake.

#### 5.5.2 Eigenvalue analysis corresponding to the lowest natural frequencies of P2 pier

The bending stiffness of the P2 pier corresponding to the lowest natural frequency is estimated similarly to the case in the bridge direction. Then the eigenvalue analysis is conducted to examine the lowest natural frequency.

Figs.12(a) and (b) show the 3<sup>rd</sup> and 4<sup>th</sup> mode shapes during the earthquake. The vibration of the P2 pier is dominant in the 3<sup>rd</sup> mode (10.2 Hz). This is why the natural frequency in Fig. 11(b) changed from around 13 Hz to 10 Hz. The vibration of the P4 pier is dominant in the 4<sup>th</sup> mode (14.2 Hz). This is why the natural frequency in Fig. 11(d) changed from around 13 Hz to around 14 Hz.

From Fig.12, the vibration of the P1 piers can be slightly seen in the 3<sup>rd</sup> and 4<sup>th</sup> modes. This is why the natural frequency in Fig. 11(a) splits into

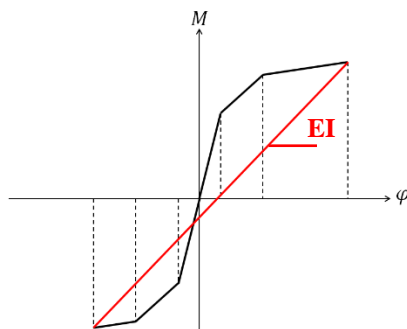


Fig.9 Estimating bending stiffness of P2 pier corresponding to the lowest natural frequency

10 Hz and 14 Hz. From Fig. 12, the vibration of the P3 pier can be seen in both the 3<sup>rd</sup> and 4<sup>th</sup> modes. Even though the deformation for the 4<sup>th</sup> mode looks larger than that for the 3<sup>rd</sup> mode, the participation factor of the 3<sup>rd</sup> mod is larger than the 4<sup>th</sup> mode. This is why the natural frequency in Fig. 11(c) splits into 10 Hz and 14 Hz.

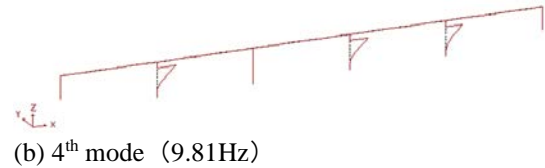
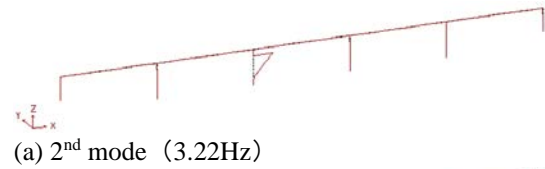


Fig. 10 Mode shape during an earthquake in the bridge direction (I-I-1, amplitude multiplied by 1)

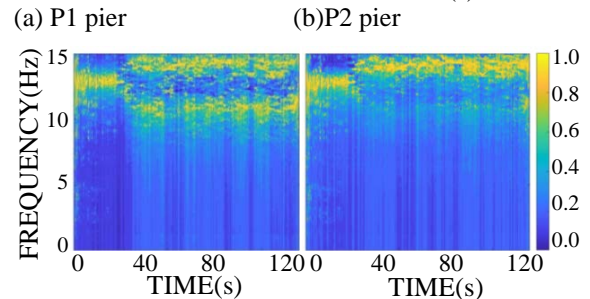
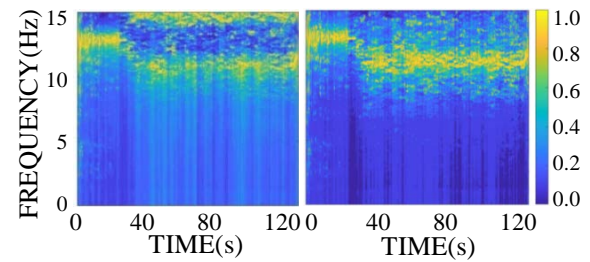


Fig. 11 NSTTF in the perpendicular direction to bridge axis (I-I-1, amplitude multiplied by 1)

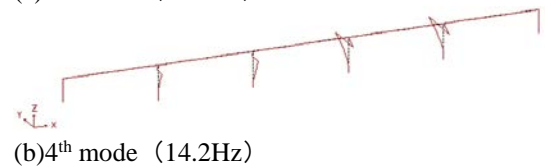
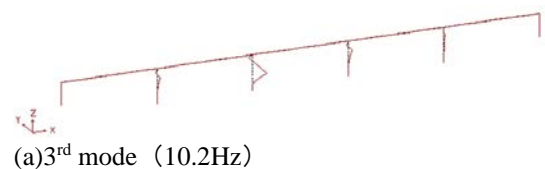


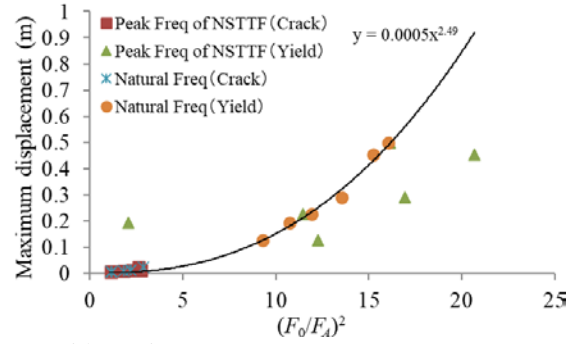
Fig. 12 Mode shape during an earthquake in the perpendicular direction to the bridge axis (I-I-1, amplitude 1x)

### 5.6 Reason for the difference between directions

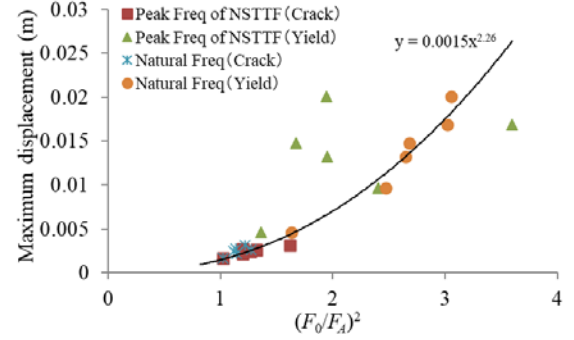
The natural frequency in the bridge axis direction (x) only changes for the damaged pier and is constant for the undamaged pier. Therefore, the proposed method can detect which pier is damaged and which is not damaged. On the other hand, the natural frequency in the direction perpendicular to the bridge axis (y) changes even for undamaged piers. Therefore, the proposed method cannot detect which pier is damaged and only can detect whether one of the piers is damaged. The reason for the difference in different directions is as follows. The girder is restrained by the bearing in the rotational direction around the x-axis. Therefore, when the P2 pier vibrates in the y direction, the P2 pier top rotates around the x-axis. It makes the girder rotate, and the top of the other piers will also rotate. Thus, the stiffness reduction of the P2 pier due to damage affects the vibration of the entire bridge. This is why the natural frequency of the undamaged piers changes. In the bridge axis direction, the P2 piers are free to rotate around the y-axis and are elastically supported in the y-axis direction. Therefore, even if the P2 pier vibrates in the bridge axis direction, the vibration is unlikely to be transmitted to other piers via the girders. Therefore, the dominant frequency of undamaged piers does not change.

### 5.7 Relationship between $(F_0/F_A)^2$ and maximum displacement

Next, the relationship between  $(F_0/F_A)^2$  and the maximum displacement is examined. The result for 12 input ground motions is shown in Fig. 13 for the P2 pier. The legend “Crack” shows the result when the P2 pier suffered cracking. The legend “Yield” shows the result when the P2 pier suffered yielding. The legend “Natural Freq” indicates the lowest natural frequency during earthquake excitation  $F_A$ , estimated by the eigenvalue analysis using the decreased bending stiffness. The plots of “Natural Freq (Crack)” and “Natural Freq (Yield)” are on one smooth curve. It shows the possibility of estimating the maximum displacement from  $(F_0/F_A)^2$  by calculating the smooth curve priori by numerical analysis. However, it is difficult to estimate  $F_A$  visually from NSTTF since the NSTTF is unclear. Therefore, we tried to read  $F_A$  automatically from the NSTTF. The legend “Peak Freq of NSTTF” indicates the lowest peak frequency at which the transfer function takes the maximum value. Unfortunately, “Peak Freq of NSTTF” and “Natural Freq” does not match since the transfer function does not necessarily take its maximum value at the natural frequency. Therefore, the method to automatically and accurately read  $F_A$



(a) Bridge axis



(b) Perpendicular to bridge axis

Fig. 13 Relationship between  $(F_0/F_A)^2$  and maximum displacement for P2 pier

from the NSTTF is necessary.

If it becomes possible to estimate  $F_A$  from NSTTF, estimating the maximum displacement from  $(F_0/F_A)^2$  becomes possible by calculating the relationship between  $(F_0/F_A)^2$  and the maximum displacement priori.

## 6. CONCLUSIONS

This study investigated the damage assessment method for RC piers through the numerical analysis of the entire bridge. The following are the findings of this study.

- 1) In the bridge axial direction, the natural frequency of the damaged P2 piers decreased due to the damage, while the natural frequencies of the undamaged piers remained unchanged. Therefore, detecting which pier is damaged and undamaged is possible.
- 2) In the direction perpendicular to the bridge axis, not only the natural frequency of the damaged P2 pier but also the natural frequency of the undamaged piers changed. It is possible to detect that one of the piers is damaged, but it is not possible to detect which pier is damaged.
- 3) The reason for the different trends between the different directions could be explained based on the support conditions of the bearings.
- 4) The plot of the relationship between  $(F_0/F_A)^2$  and the maximum displacement resulted in a smooth, monotonically increasing curve.

Therefore, estimating the curve priori may make it possible to estimate the maximum displacement from the lowest natural frequency during excitation  $F_A$ .

- 5) The method to automatically estimate the lowest natural frequency  $F_A$  from the NSTTF needed to be developed.

This study assumed the damage to the pier. In future studies, we would like to consider damage to other members, such as bearings [14,15] and cables [16,17].

## 7. ACKNOWLEDGMENTS

This work was supported by JSPS KAKENHI Grant Number 22K18830.

## 8. REFERENCES

- [1] NILIM-PWRI Joint Reconnaissance Team for the Mid Niigata Prefecture Earthquake in 2004, Report on damage to infrastructures by the Mid Niigata Prefecture earthquake in 2004. Proc. of the 37th Joint Meeting of U.S.-Japan Panel on Wind and Seismic Effects/UJNR, Technical Note of NILIM, 2005, pp.1-21. <https://www.pwri.go.jp/eng/ujnr/joint/37/paper/21matsuo.pdf> (last viewed on August 25, 2023)
- [2] Hu Y., Arakaki T., Oeda Y., Study on the influence and recovery process in the Kumamoto Earthquake on the functional deterioration of wide area road network in Kyushu caused by road closure. Journal of the City Planning Institute of Japan, Vol. 53, Issue 3, 2018, pp. 852-858.
- [3] Seki, M., Nishimura, A., Sano, H., Nakano, S., Study on the evaluation of damage levels of RC rigid frame railway bridges in the case of earthquakes. Journal of JSCE, No. 731/I-63, 2003, pp. 51-64.
- [4] Nagata, S., Kanazawa, K., Kajiwara, K., Yabana, S., Seismic damage evaluation of full-scale RC bridge pier specimens based on an ambient vibration monitoring. Journal of Structural Engineering, Vol. 56A, 2010, pp. 49-59.
- [5] Kobayashi, H., Unjo, S., Kano, T., Development of an earthquake damage detection method for bridge structures with the accelerating sensor. Proceedings of the JSCE Earthquake Engineering Symposium, Vol. 28, No. 23, 2005, pp. 1-7.
- [6] Furukawa, A., Igarashi, A., Kiyono, J., Estimation of maximum response ductility using equivalent natural period and damping ratio obtained from acceleration response of a nonlinear SDOF system with bilinear hysteresis during earthquakes. Journal of JSCE, Ser. A2, Vol. 67, No. 2, 2011, pp. I\_801-I\_812.
- [7] Hida, T., Mizutani, M., Takahashi, Y., Fujino, Y., Simple damage detection technique of RC columns by wavelet transform of their acceleration responses. Journal of JSCE, Ser. A2, Vol. 70, No. 2, 2014, pp. I\_937- I\_945.
- [8] Furukawa, A., Hagiwara, K., Takahashi, Y., Kiyono, J., Quick earthquake damage evaluation method for RC piers using acceleration measurements. International Journal of GEOMATE, Vol. 21, Issue 86, 2021, pp. 23-31. <http://dx.doi.org/10.21660/2021.86.j2210>
- [9] Furukawa, A., Yagi, R., Takahashi, Y., Kiyono, J., Fundamental study on earthquake damage evaluation method for RC piers using nonstationary SDOF model. Journal of Civil Engineering Structures and Materials, Vol. 37, 2021, pp. 61-70.
- [10] Takahashi, Y., Kobayashi, N., Quantitative evaluation of seismic response based on simultaneous excitation of 16 RC columns. Journal of JSCE, Ser. A1, Vol. 72, Issue 1, 2016, pp. 176-191.
- [11] Japan road association, Materials on seismic design of road bridges. Maruzen, 1997, pp. 1-472.
- [12] ARK Information Systems, Inc., TDAP III Reference manual. 2017, pp. 1-898.
- [13] Japan road association, Specifications for highway bridges: Part V Seismic design. Maruzen, 2017, pp.1-302.
- [14] Wang Z, Zeng Q., Du Y., An W., Transient response of bridge piers under eccentric impact of near-fault earthquake. Scientific Reports, Vol. 12, Article No. 16667, 2022, pp. 1-15.
- [15] Sun G., Yuang Z., Wu B., Zhao F., Methodology and application of safety evaluation of reinforced concrete girder bridges during earthquakes. Shock and Vibration, Vol. 2022, Article ID 5591334, 2022, pp. 1-12.
- [16] Furukawa, A., Hirose, K., Kobayashi, R., Tension estimation method for cable with damper using natural frequencies. Frontiers in the built environment, Vol.7, Article 603857, 2021, pp. 1-17. <https://doi.org/10.3389/fbuil.2021.603857>
- [17] Furukawa, A., Yamada, S., Kobayashi, R., Tension estimation methods for two cables connected by an intersection clamp using natural frequencies. Journal of Civil Structural Health Monitoring, Vol. 12, 2022, pp. 339-360. <https://doi.org/10.1007/s13349-022-00548-6>